

TIME STEPPING FINITE ELEMENT ANALYSIS OF BROKEN BARS FAULT IN A THREE-PHASE SQUIRREL-CAGE INDUCTION MOTOR

J. Faiz

Faculty of Electrical and Computer Engineering
University of Tehran
Tehran, Iran

B. M. Ebrahimi and M. B. B. Sharifian

Faculty of Electrical and Computer Engineering
University of Tabriz
Tabriz, Iran

Abstract—Broken rotor bars and end-ring are common faults in three-phase squirrel-cage induction motors. These faults reduce the developed torque and increase the speed fluctuations of the motor. Meanwhile, developed unsymmetrical magnetic generates noise and vibration in the motor. Local heat around the broken bars may gradually break the adjacent bars and the motor will be finally out of service.

Finite element method (FEM) is the most accurate technique for diagnosis and analysis of induction motor, because it can include all actual characteristics of the healthy and faulty induction motors. However, current density is generally considered as input for performance computation process, while fault can inject a large harmonics to the stator current. These harmonics may not be ignored in the fault diagnosis of the motor. In addition, all FE applications consider the steady-state mode of operation.

In this paper, a three-phase voltage-fed squirrel-cage induction motor with rotor broken bars is proposed and analyzed for the starting period of the motor. Both no-load and on-load cases are considered. Also, concentrated rotor broken bars under one-pole and the distributed rotor broken bars under different poles are studied and compared.

1. INTRODUCTION

Heavy loaded induction motors particularly those that are iteratively started and stopped, exposed to the faults such as rotor broken bars and end rings which lead to asymmetry of the squirrel-cage rotor. Such faults disturb operation of the motor and shorten its lifetime. Therefore, diagnosis and detection of faults in induction motors can preserve good performance of the motor and its normal lifetime [1]. The basis of any reliable diagnosis method is inclusion of the real behaviors and conditions of a faulty motor. At this end, a proper modeling is the first step in this process. A model that could include discrete stator windings distribution, magnetic non-linearity of the core, used elements in the motor, slots and rotor bars, topology of the motor structure and spatial and time harmonics is a convenient model for a faulty diagnosis of induction motors.

The initial steps in fault detection were based on the measurement of speed oscillations, noise and stray flux which had low reliability. Until 1987, there was limitation on the type and degree of fault and no general and wide spread technique was available to study a faulty induction motor with different number of rotor broken bars and pole number. Norton theorem was used in [2] to analyze an induction motor with broken rotor bar. However, in [2], it has been assumed that there is no coupling between rotor and stator and just the rotor cage behavior in air gap has been investigated. The inter-bars current in the broken bar rotor was considered in [3], where it was assumed that the induced voltage in broken bar and two surrounded bars have the identical amplitude and phase angle, while this assumption is only acceptable if a large number of poles present, not in two-pole motors. The test on a faulty induction motor shows that the inter-bar current generates axial vibration with speed equal to 4 times the rated speed of the motor [4] which is applicable for fault diagnosis. Estimation and measurement of the apparent resistance of the broken bar has been suggested for fault diagnosis [5]. This has been done off-line which reduce the accuracy of the method [5]. Magnetic asymmetry is visible on both d and q components of the stator currents, while the load fluctuations affects only on the q component [6]. It is noted that dq model of induction motor unable to include all fault assumptions, because dq transformations have not taken into account spatial and time harmonics and relationship and the effects of these harmonics upon the leakage fluxes, magnetic inductance, currents, torque, ohmic losses and core losses [7, 8]. Winding function has been employed in healthy and broken bar induction motor [9]. Normally, symmetrical air gap has been assumed in the application of winding function method

[10,11]; however, the basic equation has been revised in [12] and indicated that the winding function method for uniform and non-uniform air gap differ.

Diagnosis and analysis methods of induction motors using old model, lumped parameters and winding function method have two basic drawbacks. The first is a modeling algorithm that addresses the lack of comprehensive field fault data bases. The second is an algorithm that addresses the difficulty in distinguishing between degrees of faults [13]. A proper and accurate method that has been suggested to resolve this is application of finite element method (FEM). The reasons are that having precise magnetic field distribution and performance of motor make it possible to predict performance of the faulty motor due to the change of parameters [14]. The FEMs are also based on the magnetic field distribution and are suitable tools for analysis of faulty induction motors considering complicated and non-linear behavior of the motor. Field distribution within induction motor with five broken bars has been determined in [15]. An induction motor with a broken bar has been analyzed using time stepping finite element method in [16]. One difficulty in analysis of a faulty induction motor by the FEM is that current density in any region is considered as input of equations. This is possible for the proposed steady-state case where current harmonics are ignored, but in the case of rotor broken bars, there are a large number of injected harmonics to the stator current and it is impossible to neglect them. Therefore, the current density of different windings must be calculated using alternative method. This method has been proposed as time stepping finite element coupled state-space method [17–21]. This method estimates the inductances of the motor using the TSFE method, and solutions are inputs of the state-space section. Following the state-space equations, the solutions of this section are considered as inputs of the FEM. This is the trend for achieving the convergence.

For simulation using the TSFE-SS method, the initial values of rotor current and angular position must be estimated, the numerical convergence of winding currents depend on the proper estimate of these values. It is particularly true when an inverter model under no-load and full load is simulated. Meanwhile, in this method the FE is only used to evaluate inductances of the motor; the rest of computations and analyses are carried out using state-space equations. Finally, the influence of broken bars distribution in different poles has not been considered while this effect differs for concentrated and distributed broken bars.

This paper presents a solution for the above-mentioned problems. At this end, a very precise and suitable model containing the spatial

and time harmonics, magnetic saturation, stator winding distribution, effects of rotor slots and topology of the non linear magnetic circuits are presented. A faulty voltage-fed induction motor is analyzed and diagnosed in this paper. In this case, terminal voltages are accounted for input values and output current are computed. Therefore, in addition to a very accurate computation all problems due to coupling between two FE and state-space softwares are removed.

FEMs have been so far applied to the steady-state analysis of faulty induction motor. However, if induction motor does frequently starts and stops, breakage of rotor bars is possible in the restarting case. Meanwhile, there are some problems such as noise, large UMP and even arcing during starting of rotor broken bars case. This is the reason for the analysis of rotor broken bar induction motor from stall up to the steady-state mode.

Finally, transient analysis of broken-bar induction motor from starting up to the steady-state conditions for no-load and on-load cases are given.

2. ROTOR BROKEN BARS

Cracked or broken rotor bars and end-ring are common faults in three-phase squirrel-cage induction motors. Rotor bars faults are often occurred more than that of molded rotor. The former rotor bar can be easily repaired. The temperature rise around the cracked bars can eventually break the bars and electric arc produces around broken bars region. This can damage the laminations of the rotor body close to the broken bars region. This is the reason for passing the broken bar current from the adjacent bars, and these adjacent bars transfer larger current and generate a larger stress. Therefore, a new stage of cracking begins; for this reason when a rotor bar is broken, the adjacent bars are opposed on a fault due to large applied stress. It means following the first broken bar and after a short period, other bars may be broken [22]. The following reasons can lead to cracking or broken rotor bars [23]:

1. Thermal stress due to over-load, non-uniform heat distribution, hot spot and arc.
2. Magnetic stresses due to electromagnetic forces, magnetic asymmetry forces, noises and electromagnetic vibrations.
3. Residual stress from the fabrication process.
4. Dynamic stress due to rotor axial torque and centrifugal forces.
5. Circumferential stress due to wearing and pollution of rotor material by chemical materials and humidity.

6. Mechanical stress due to mechanical fatigue of different parts, ball-bearing damage, loosens laminations etc.

Figure 1 shows two distributed models and cage rotor in a healthy motor. As shown, two adjacent bars form a loop. Fig. 2 shows the distributed model of rotor cage when a rotor bar has been broken. As shown, the currents of two loops consisting the proposed bar, are identical.

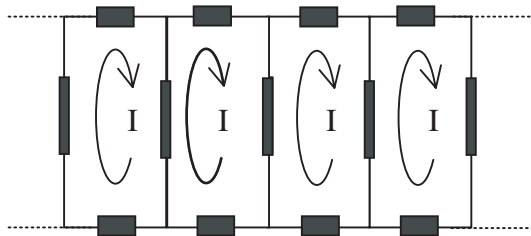


Figure 1. Distributed rotor cage in healthy induction motor.

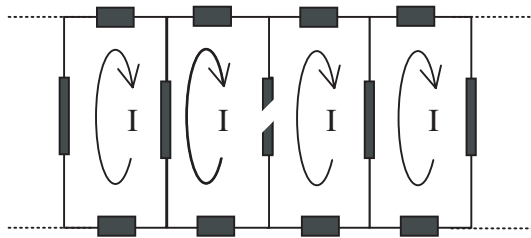


Figure 2. Distributed rotor cage in induction motor with one broken rotor bar.

3. TRANSIENT ANALYSIS OF A FAULTY INDUCTION MOTOR

The FEM can be used for steady-state analysis of induction motor in the eccentricity condition. It is also possible to analyze the transient behavior of induction motor by the FEM. This is required in the control of induction motor in order to obtain the optimal time response. Meanwhile, the transient analysis of the motor is required for on-line fault diagnosis of the motor.

A voltage-fed three-phase induction motor is analyzed from stall up to the steady-state mode in which the continuous motion of rotor

is considered using the TSFE method. The FE matrix equations, electric circuit equations and electromechanical equations are solved every step. The couple solver part of Opera-2d is used in order to allow the user to study the transient behavior of the motor.

There are three fundamental parts in the transient analysis of induction motor: (1) modeling of motor, (2) connecting electrical circuits and supply modeling, and (3) electromechanical connections.

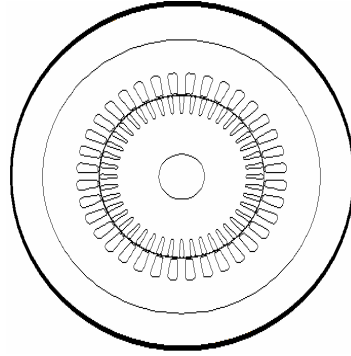


Figure 3. Cross-section of proposed induction motor.

3.1. Modeling Squirrel Cage Induction Motor

The proposed three-phase squirrel-cage induction motor, with cross-section shown in Fig. 3, is modeled taking into account the properties of the various parts including stator, rotor, shaft, rotor bars and air gap. Meanwhile, a special attention is paid to the moving parts of the motor, because magnetic forces and positions influence, in turn, the magnetic field within the motor. In the model, the voltage is applied as input and the total current is the unknown value. The transient equations of the external circuit that show the electrical supply and circuit elements are combined with the equations of the FEM. Also the motion equations are combined with the field equations of the FEM. Finally, in the moving electromagnetic systems, it is necessary to introduce the speed in the equations. The equation which covers this section is as follows:

$$\nabla \times \left(\frac{1}{\mu} \vec{V} \times \vec{A} \right) + \sigma \left(\frac{\partial \vec{A}}{\partial t} - \vec{v} \times (\nabla \times \vec{A}) \right) = \vec{J} \quad (1)$$

Using a reference frame which is assumed constant under the study

part, the relative speed v is expressed as follows:

$$\nabla \times \left(\frac{1}{\mu} \nabla \times \vec{A} \right) + \sigma \left(\frac{\partial \vec{A}}{\partial t} \right) = \vec{J} \quad (2)$$

In the FE analysis, such reference frame is created by placing a mesh on the surface of the moving part and movement or transformation occur only within the elements that are placed around the moving element [20].

3.2. Connection of Electrical Circuits and Supply Modeling

All rotor bars and stator conductors that have been presented in the circuit model are shown using the real constants in the FEM. Additional resistance and inductance place in series with the every phase of the winding. The induction motor is supplied by a three-phase sinusoidal supply. Rotor bars in the relevant circuit are in parallel. Three stator windings of phases a , b and c have identical turns number and resistances. Three-phase symmetrical voltages are applied to the stator. The two-dimensional propagation equation is as follows:

$$\nabla \times \vec{v} \nabla \times \vec{A} = \vec{J} \quad (3)$$

where J and A are taken to be in z direction and independent of z . The current density is as follows:

$$\vec{J} = \sigma \frac{\vec{V}_b}{l} - \sigma \frac{\partial \vec{A}}{\partial t} + \sigma \vec{v} \times \vec{B} \quad (4)$$

where the amplitude of gradient of V_b in z direction is V_b/l . Fig. 4 shows the physical interpretation of V_b .

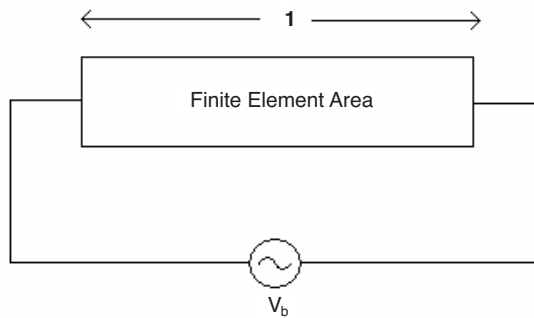


Figure 4. Physical interpretation of V_b .

The first term in the right hand side of (4) shows the current density due to the power supply. The second term shows the induced current density and the third term indicates the produced current density by the series voltage. It is not possible to separate its different parts experimentally due to mathematical concept of (4). Therefore, the time-dependent magnetic propagation equation is as follows:

$$\nabla \times \vec{v} \nabla \times \vec{A} = \sigma \frac{\vec{V}_b}{l} - \sigma \frac{\partial \vec{A}}{\partial t} + \sigma \vec{v} \times \nabla \times \vec{A} \quad (5)$$

Using a reference frame which is considered constant in respect with the studied element, the relative speed v is zero and (5) is simplified as follows:

$$\nabla \times \vec{v} \nabla \times \vec{A} = \sigma \frac{\vec{V}_b}{l} - \sigma \frac{\partial \vec{A}}{\partial t} \quad (6)$$

For combining the circuit and field equations, it is necessary to calculate the total current of every conductor. This is done by integration of (6) over the cross-section of the conductor as follows:

$$i = \iint \left(\sigma \frac{V_b}{l} - \sigma \frac{\partial A}{\partial t} \right) dx dy \quad (7)$$

The total current of every conductor is related to the voltage supply through lumped resistance R_{ext} and inductance and L_{ext} . So the time-dependent circuit equation that expresses this relationship is determined. The basic element of a circuit is a bar that is defined as an individual conducting region having length l in z direction. A series connected bars forms the coils. These coils can be connected in parallel.

Suppose bars b_1, b_2, \dots, b_n are connected in series to form a coil. All bars in a coil carry the total current, but the successive bars carry this current in the opposite direction. Two ends of the coil leave the FE region and are connected to the voltage source. Resistance and reluctance from these two ends are modeled by lumped resistance R_{ext} and inductance L_{ext} .

The applied voltage to the external terminals of coil is V_c and terminal voltage in the FE region is v_t . The voltages of the bars that form the coils (means for coil C) are:

$$V_{t,c} = \sum_{b \in c} d_b V_b \quad (8)$$

where d_b is equaled to +1 or -1 and it shows the polarity of bar b . In Fig. 4, bar 1 is positive, bar 2 is negative, \dots , V_b has been shown in Fig. 3. Therefore:

$$V_c = \{d_b\}_c^T \{V_b\}_c + L_{ext}(di_c/dt) + R_{ext}i_c \quad (9)$$

It means that this equation is used to relate the FE region with V_b characteristic to external circuits and sources with R_{ext} , L_{ext} and V_c .

If the coils are connected in parallel, an individual circuit forms in the output terminals of the system. The general case consisting of connection of P coils in parallel with supply V_s , internal resistance R_s and inductance L_s has been shown in Fig. 5. The governing RL

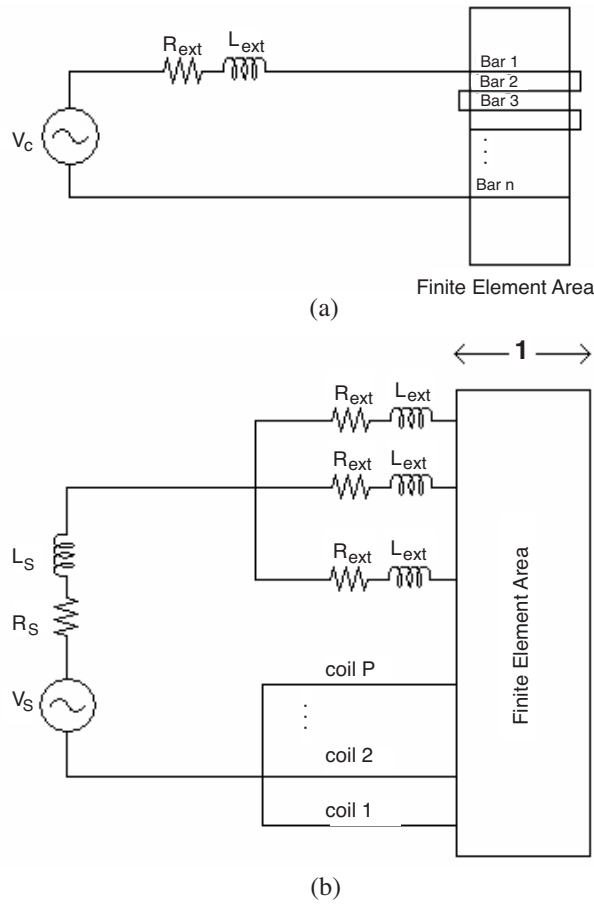


Figure 5. Forming coils: (a) series bars, (b) parallel bars.

equation of this combination is as follows:

$$V_s = R_s^T \sum i_c + L_s \sum di_c/dt + V_c \quad (10)$$

And its matrix form is:

$$V_s = R_s \{1\}^T \{i\}_c + L_s \{1\}^T \{di/dt\}_c + V_c \quad (11)$$

where $\{i\}$ is the column matrix with dimension P and all elements are 1. In general system of equations, for every set of parallel coils, there is an equation similar to (11). So the developed electromagnetic torque of the motor is as follows:

$$T_e = (L_{eff}/\mu_0) \int_{\Gamma} \left[\left(\vec{B} \cdot \vec{n} \right) \left(\vec{r} \cdot \vec{B} \right) - 0.5 B^2 \left(\vec{r} \times \vec{n} \right) \right] d\Gamma \quad (12)$$

where, \vec{n} is the unit vector normal to the contour, \vec{r} is the vector pointing from the axis rotation to a point on the contour. The discrete developed electromagnetic torque is obtained as follows:

$$T_e = (2L_{eff}r^2/\mu_0) \sum_{i=1}^n B_{ri} B_{\theta i} \Delta\theta_i \quad (13)$$

where r is the radius of the contour, n is the number of elements passed the contour over a pole pitch, B_r and B_{θ} is the normal and tangential component of the magnetic flux density respectively in each element.

3.3. Electromechanical Connections

The induction motor motion equation can be expressed as follows:

$$T_e - T_l = j(d\omega_r/dt) + B_m\omega_r \quad (14)$$

$$\omega_r = d\theta/dt \quad (15)$$

The on-load faulty induction motor increases the unsymmetrical magnetic torque that increases unbalanced magnetic pull (UMP), level of noise and vibration. This particularly sensible in the steady-state mode. This is the reason for analysis of faulty on-load induction motor from stall up to the steady-state mode.

Damping factor and friction torque have been also included in this paper. The friction torque consists of friction between the shaft, and flange or bal-bearing and different parts of the load. Its value at stall is larger than that very low speed. Velocity of torque is presented by $B_m\omega_r$. The load torque includes a part of the torque that is useful in developing work. Characteristic of the load torque depends on the load type and its application. This is taken to be fixed here and equal to the rated torque of the motor.

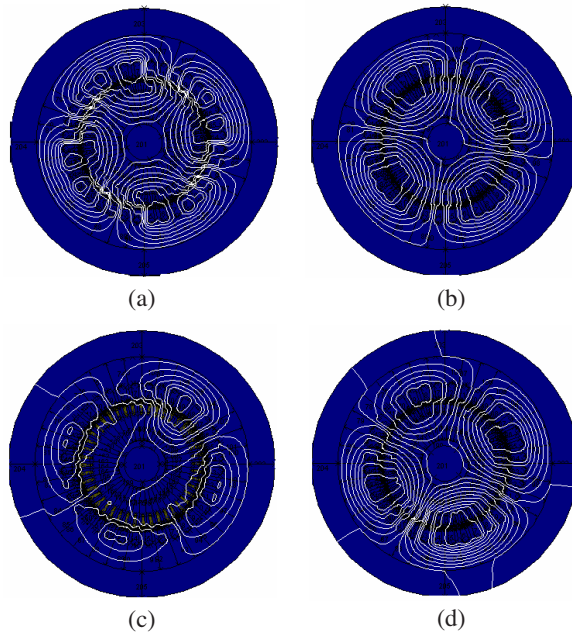


Figure 6. Flux distribution: (a) beginning of healthy motor starting, (b) steady-state operation of healthy motor, (c) beginning of faulty motor starting, (d) steady-state operation of faulty motor.

4. RESULTS

Figure 6 shows the magnetic flux distribution in the starting and steady-state mode of induction motor operation for healthy and broken bars. The reasons for asymmetry of the flux lines are eddy current particularly in the slots of the rotor, sever changes of slip at the beginning of starting period and very high starting current (Fig. 6(a)). In addition injected harmonic currents and saturation due to the broken bars also cause asymmetry of the flux lines (Fig. 6(c)). When the healthy induction motor approaches the steady-state, the flux lines are more symmetrical distributed (Fig. 6(b)), while in broken bar motor the flux lines distribution are still unsymmetrical in the steady-state mode (Fig. 6(d)). Fig. 7(a) shows time variations of phase a current for the three-phase healthy motor and no-load starting. At the starting the current, flux and flux density are high and core saturates. If magnetization characteristic has not been included in the analysis of the starting of the motor, the teeth potential increases considerably. This leads to a large electromagnetic torques at the

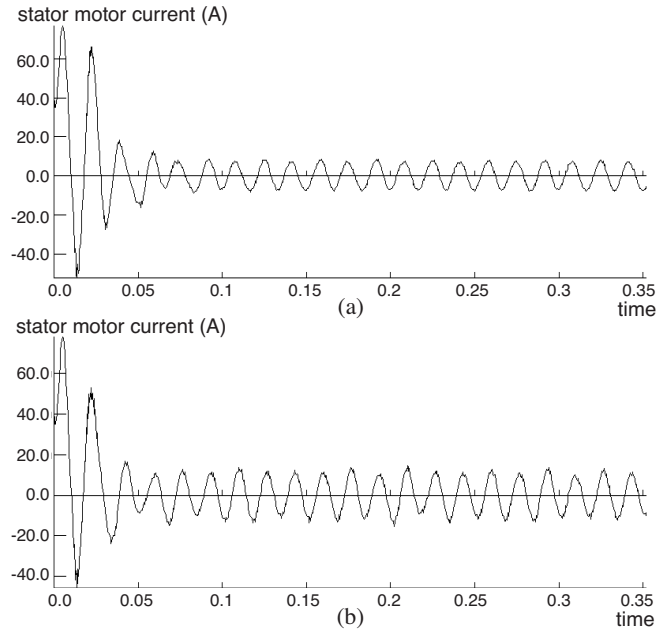


Figure 7. Time variations of current of a healthy induction motor: (a) without load, (b) with full load.

starting instant. However, analysis of the starting of the motor including the magnetization characteristic considerably reduces the developed torque compared with the constant permeability. In both cases the rate of the torque variations is large due to the quick changes of the slip at the beginning of the starting. Fig. 8 exhibits time variations of the torque, of a healthy no-load induction motor. The current of the bar just before the break passes the adjacent bars just after bar break. In addition to a deeper saturation of the core and the injected harmonics to the current, the *rms* currents in the bars adjacent to the broken bar increase. However, raise of the broken bars leads to more serious problems in the motor. Figs. 9(a) and 10(a) show the time variations of the current for 1 and 6 broken bars respectively. More broken bars lead to more asymmetry of the magnetic flux density distribution which causes quick variations of the torque profiles (Figs. 11(a) and 12(a)). Starting of an on-load induction motor differs with that of the no-load motor. The starting period in this case is shorter than that of the no-load case. Meanwhile, instantaneous current, torque and speed at no-load are comparable with that of the full-load case. At the same time, difference between

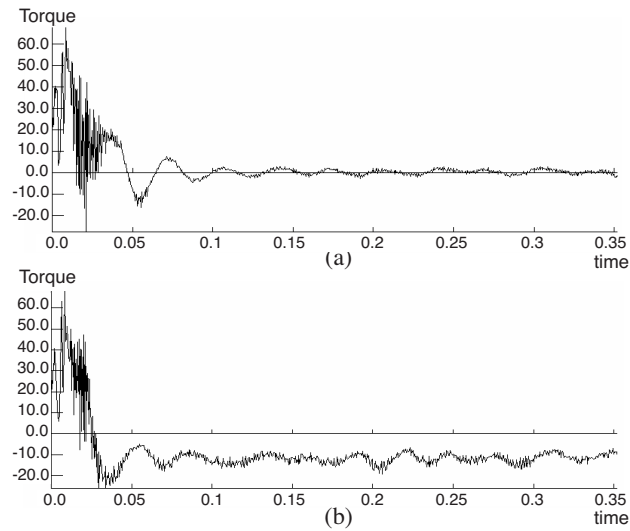


Figure 8. Time variations of torque of a healthy induction motor: (a) without load, (b) with full load.

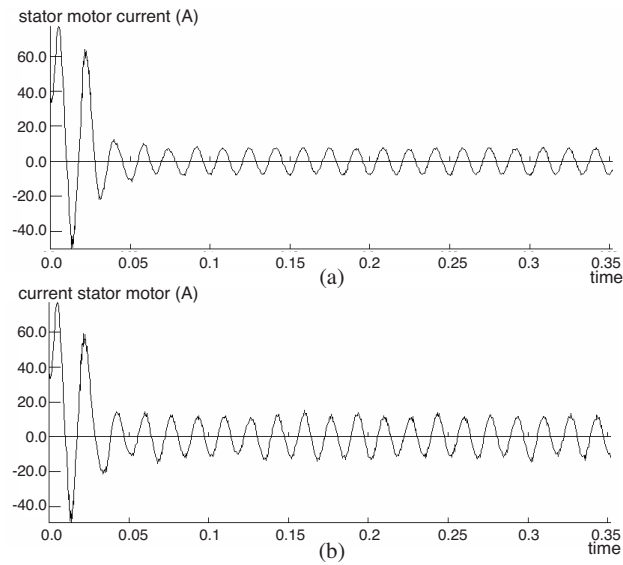


Figure 9. Time variations of current of a faulty induction motor, with 1 broken bar: (a) without load, (b) with full load.

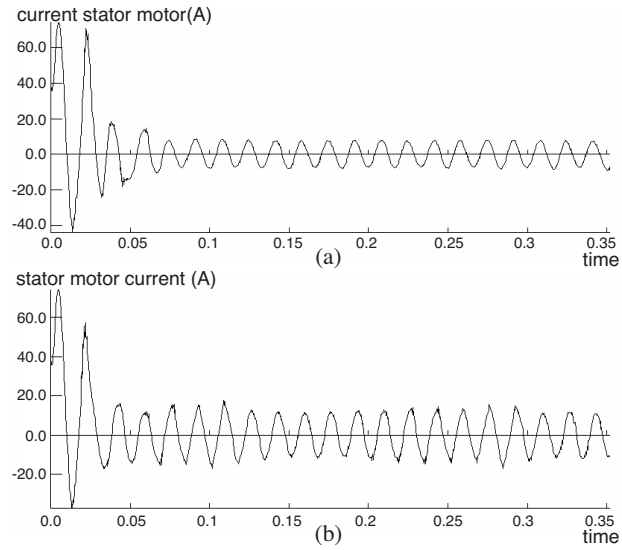


Figure 10. Time variations of current of an induction motor, with 4 broken bars: (a) without load, (b) with full load.

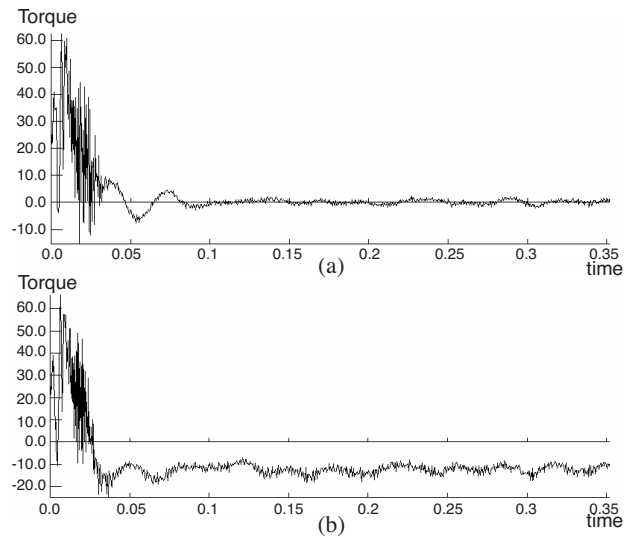


Figure 11. Time variations of torque of a faulty induction motor, with 1 broken bar: (a) without load, (b) with full load.

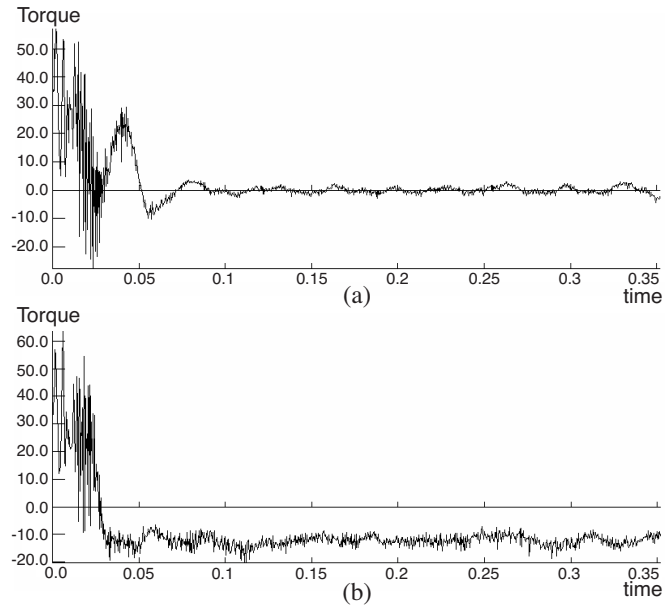


Figure 12. Time variations of torque of a faulty induction motor, with 4 broken bars: (a) without load, (b) with full load.

their steady-state cases is clearer. Fig. 7(b) show the time variations of a healthy on-load induction motor at starting. Figs. 9(b) and 10(b) exhibit the time variations of the on-load induction motor with 1 and 6 broken bars. Since the motor has been started on-load the steady-state torque must be equal to the rated speed (Figs. 11(b) and 12(b)).

5. CONCLUSIONS

This paper analyzed a broken-bar voltage-fed three-phase squirrel-cage induction motor in transient case. The basic problem with the FEMs in the analysis of a faulty induction motor is high contents of the harmonics in the stator current, and this leads to calculation of the windings current such that more complicated FE computations required. Meanwhile, using voltage-fed induction motor in this paper resolved all the difficulties. It is noted that this paper considered the transient mode of operation of a faulty motor. Therefore electromagnetic torque versus speed has been obtained which was not determined in the previous work where only steady-state case was studied. The influence of the broken bars upon the speed profiles of the motor was determined.

It has been shown that in broken bars motor the stator current characteristics and the torque are sensibility varied. The speed profiles oscillate due to the broken bars and the settling time becomes shorter.

REFERENCES

1. Bonnett, A. H. and G. C. Soukup, "Cause and analysis of stator and rotor failures in three-phase squirrel-cage induction motors," *IEEE Trans. on Industry Applications*, Vol. 28, No. 4, 921–937, July–Aug. 1992.
2. Deleroi, W., "Squirrel cage motor with broken bar in the rotor-physical phenomena and their experimental assessment," *ICEM*, 767–770, Budapest, 1982.
3. Kerzenbaum and C. F. Landy, "The existence of large inter-bar currents in three phase squirrel cage motors with rotor-bar and/or end ring faults," *IEEE Trans. on Power Apparatus and Systems*, Vol. 129, Part. B, No. 3, 767–770, 1982.
4. Landy, C. F. and R. More, "Further success in the detection of broken and/or cracked rotor bars in large squirrel cage induction motors," *Proc. IEE Int. Conf. EMD.*, 145–149, 1987.
5. Cho, K. R., J. H. Lang, and S. D. Umans, "Detection of broken bars in induction motor using state and parameter estimation," *IEEE Trans. Industry Applications*, Vol. 28, No. 3, 702–709, May/June 1992.
6. Schoen, R. R. and T. G. Habetler, "Effects of time varying loads on rotor fault detection in induction machines," *IEEE IAS 93*, 324–330, 1993.
7. Demerdash, N. A., J. F. Bangura, and A. A. Arkadan, "A time-stepping coupled finite element-state space model for induction motor drives, I. Model formulation and machine parameter computation," *IEEE Trans. on Energy Conversion*, Vol. 14, No. 4, 1465–1471, Dec. 1999.
8. Bangura, J. F., F. N. Isaac, N. A. Demerdash, and A. A. Arkadan, "A time-stepping coupled finite element-state space model for induction motor drives, II. Machine performance computation and verification," *IEEE Trans. on Energy Conversion*, Vol. 14, No. 4, 1472–1478, Dec. 1999.
9. Toliyat, H. A. and T. A. Lipo, "Transient analysis of cage induction machines under stator, rotor bar and end ring faults," *IEEE Trans. on Energy Conversion*, Vol. 10, No. 2, 241–247, June 1995.
10. Joksimovic, G. M., M. D. Durovic, J. Penman, and N. Arthur,

- “Dynamic simulation of dynamic eccentricity in induction machines-winding function approach,” *IEEE Trans. on Energy Conversion*, Vol. 25, No. 2, 143–149, June 2000.
11. Toliyat, H. A., M. S. Arefeen, and A. G. Parlos, “A method for dynamic simulation of air-gap eccentricity in induction machines,” *IEEE Trans. on Industry Applications*, Vol. 32, No. 4, 910–918, July 1996.
 12. Faiz, J. and I. Tabatabaei, “Extension of winding function theory for non uniform air gap in electric machinery,” *IEEE Trans. on Magnetism*, Vol. 38, Issue 6, 3654–3657, Nov. 2002.
 13. Bangura, J. F., R. J. Povinelli, N. A. O. Demerdash, and R. H. Brown, “Diagnostics of eccentricities and bar/end-ring connector breakages in poly phase induction motors through a combination of time series data mining and time-stepping coupled FE-state-space techniques industry applications,” *IEEE Trans. on Industry Applications*, Vol. 39, Issue 4, 1005–1013, July–Aug. 2003.
 14. Fisher, R., “Application of a finite element method to predict damage induction motor performance,” *IEEE Trans. on Magnetism*, Vol. 37, No. 5, 3635–3639, Sep. 2001.
 15. Elkasabgy, N. M., A. R. Eastham, and G. E. Dawson, “Detection of broken bars in the cage rotor on an induction machine,” *IEEE Trans. on Industry Applications*, Vol. 22, No. 6, 165–171, 1992.
 16. Kim, C. E., Y. B. Jung, S. B. Yoon, and D. H. Im, “The fault diagnosis of rotor bars in squirrel cage induction motors by time-stepping finite element method,” *IEEE Trans. on Magnetism*, Vol. 33, Issue 2, Part 2, 2131–2134, March 1997.
 17. Bangura, J. F. and N. A. Demerdash, “Diagnosis and characterization of effects of broken bars and connectors in squirrel-cage induction motors by a time-stepping coupled finite element-state space Modeling approach,” *IEEE Trans. on Energy Conversion*, Vol. 14, Issue 4, 1167–1176, Dec. 1999.
 18. Bangura, J. F. and N. A. O. Demerdash, “Effects of broken bars/end-ring connectors and air gap eccentricities on ohmic and core losses of induction motors in ASDs using a coupled finite element-state space method,” *IEEE Trans. on Energy Conversion*, Vol. 15, Issue 1, 40–47, March 2000.
 19. Povinelli, R. J., J. F. Bangura, N. A. O. Demerdash, and R. H. Brown, “Diagnostics of bar and end-ring connector breakage faults in poly phase induction motors through a novel dual track of time-series data mining and time-stepping coupled FE-state space modeling electric machines and drives,” *IEEE International*

- Conference IEMDC*, 809–813, 2001.
20. Povinelli, R. J., J. F. Bangura, N. A. O. Demerdash, and R. H. Brown, “Diagnostics of bar and end-ring connector breakage faults in poly phase induction motors through a novel dual track of time-series data mining and time-stepping coupled FE-state space modeling,” *IEEE Trans. on Energy Conversion*, Vol. 17, Issue 1, 39–46, March 2002.
 21. Nandi, S., R. Bharadwaj, H. A. Toliyat, and A. G. Parlos, “Study of three phase induction motors with incipient rotor cage faults under different supply conditions,” *Proceedings of the IEEE-IAS Annual Meeting*, Vol. 3, 1922–1928, 1999.
 22. Toliyat, H. A. and T. A. Lipo, “Analysis of concentrated winding induction machines for adjustable speed drive applications part 1: motor analysis,” *IEEE Trans. on Energy Conversion*, Vol. 6, No. 4, 679–683, Dec. 1991.
 23. Mc Cully, P. J. and C. F. Landy, “Evaluation of current and vibration signals for squirrel cage induction motor condition monitoring,” *Proceedings of 8th Int. Conf. on Electrical Machines and Drives*, 331–335, 1997.